Kármán vortex shedding in the wake of a 2D hydrofoil: Measurement and numerical simulation

Philippe Ausoni* ✉, Mohamed Farhat*, Youcef Ait Bouziad*, Jean-Louis Kueny*, François Avellan*

* Ecole polytechnique fédérale de Lausanne
Laboratory for Hydraulic Machines
Av. Cour 33bis, 1007 Lausanne, Switzerland

✉ philippe.ausoni@epfl.ch
Phone: +41 21 693 42 78
Fax: +41 21 693 35 54

ABSTRACT

The present study deals with the shedding process of the Kármán vortices at the trailing edge of a 2D hydrofoil at high Reynolds numbers. Investigations are performed in order to evaluate the ability of an unsteady numerical simulation to accurately reproduce the vortex shedding frequency.

The vortex shedding frequency, derived from flow induced vibrations measurements, is found to follow the Strouhal law as long as none of the resonance frequencies of the hydrofoil is excited. For such lock-off conditions, the Kármán vortices exhibit a strong spanwise 3D instability. For Reynolds numbers ranging from 35'000 to 40'000, the torsion mode of the hydrofoil is excited with a substantial increase of the vibration level. In this case, the shedding frequency is locked onto the vibration frequency.

The vortex roll-up, shedding and advection are well predicted by the computations as well as the 3D instability. Nevertheless, the numerical simulations underestimate the vortex shedding frequency of about 20%. No significant influence of the turbulence models, the incoming flow turbulence intensity and the mesh size is observed on the computed values. To investigate the issue of discrepancy between absolute values of measured and computed shedding frequency, we intend to address the sensitivity of the vortex shedding frequency to the boundary layer. It is indeed know that the boundary

layer transition point to turbulence for this profile geometry is located slightly downstream of the midchord for an incidence angle of 0°. In contrast, the numerical simulation, as it solves the RANS equations, models the whole flow as being turbulent. Consequently, rough stripes are placed just behind the hydrofoil leading edge. For such a configuration, the boundary layer is turbulent from the leading edge in a similar way to the computations. Notable influence of the roughness is observed: The vortex shedding frequencies are significantly decreased in comparison to the smooth leading edge. The average Strouhal number *St* decreases from 0.24 to 0.18 and is nearly equal to the computational one, *St*=0.19. Kármán vortices being very sensitive to the boundary layer, differences in the transition points between experiments and computations have to be minimized in order to aspire good agreement.

INTRODUCTION

Placed in a fluid stream, bluff bodies generate separated flow over a substantial proportion of their surface that extends to their wake. The detachment of the boundary layers on both upper and lower surfaces forms two shear layers generating, above critical values of Reynolds number, a periodic array of discrete vortices termed Kármán street. In a range of upstream velocity, the vortex shedding frequency is known to follow the Strouhal law. From a hydrodynamic point of view, the instability of the shear layer separating from a circular cylinder has been extensively investigated; see Williamson [19] for a comprehensive review. Many authors observe that the wake structure may exhibit 3D aspect even if the obstacle and the upcoming flow are 2D. Gerrard [10] observes curved vortices and suspects that the cylinder end conditions might be the cause. Gerich *et al.* [8], Prasad *et al.* [13] and Williamson [18] find that the spanwise end conditions control the primary vortex shedding and significantly affect the stability of the separating shear layer. The influence of the surface roughness on the vortex shedding frequency in the wake of a cylinder is investigated by Achenbach *et al.* [1]. They find that very smooth surface cylinders have more chaotic and disorganized wake than for the rough surfaces. They also evidence that the Strouhal number is as high as 0.5 for the smooth cylinder, while it is 0.20 for rough surfaces.

Vortex induced vibration and fluid-structure interaction phenomena have been the issue of many researches, which Rockwell [14] and Williamson *et al.* [20] have reviewed. It is well known that the bodies which shed spanwise vortices may be excited into oscillation by the fluctuating side forces that such vortices produce. For instance, the resonance

occurs when the vortex shedding frequency coincides with one of the eigen frequencies of the combined fluid-structure system. In the case where the response amplitude becomes sufficiently large, the structural displacement can control the fluid excitation leading to the so-called “lock-in” phenomenon. The vortex shedding frequency is therefore “locked” onto the structural eigen frequency on a free velocity range.

When the pressure is low enough, bubbles filled with vapour and gas are initiated and persist in the centre of individual shed vortices. Young *et al*. [21] and Belahadji *et al*. [4] investigate the case of a flow around wedges. They observe that the cavitation development in the wake increases the shedding frequency by up to 25%. Therefore the cavitation does not constitute a passive agent for the visualization of the turbulent wake flow.

Although the Kármán vortex street has been extensively studied for flow around cylinders or wedges, only few works are related to evaluate the ability of an unsteady numerical simulation to reproduce the Kármán vortex street behind a 2D hydrofoil. The sensitivity of the vortex shedding frequency to the hydrofoil vibration and the leading edge roughness is experimentally pointed out.

CASE STUDY AND EXPERIMENTAL SETUP

The EPFL high-speed cavitation tunnel, outlined on Figure 1, is a closed loop with a test section of 150x150x750 mm, Avellan *et al.* [3]. The operating flow parameters are the upstream velocity C_{ref}, the static pressure in the test section p_{inlet} and the hydrofoil incidence angle α.

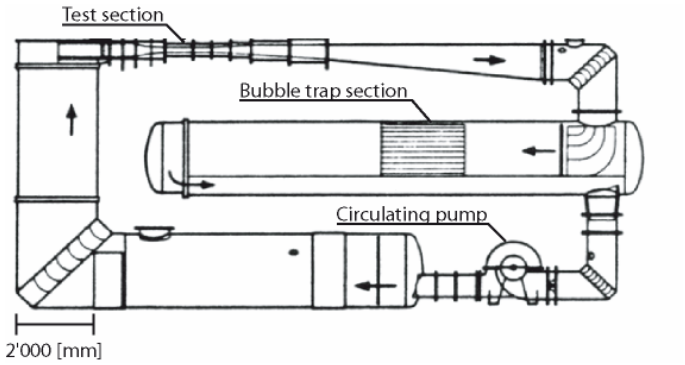

Figure 1 : EPFL high speed cavitation tunnel

The experimental 2D hydrofoil, sketched on Figure 2, is a blunt truncated Naca 0009 made of stainless steel. The trailing edge thickness *h* is 3.22 mm and its chord length *L* and span *b* are 100 mm and 150 mm respectively. For all the measurements, the

incidence angle of the hydrofoil α is fixed at 0°. The hydrofoil mounting in the test section can be considered as a perfect embedding on one side and pivot embedding on the other, Figure 2.

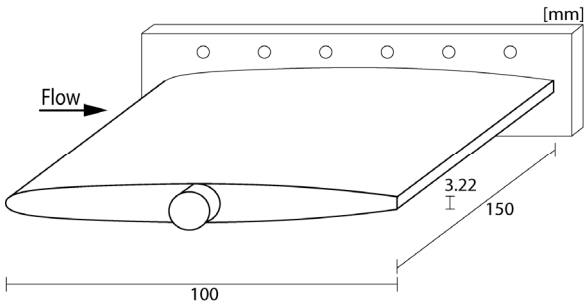

Figure 2 : Mounting of the Naca 0009 hydrofoil in the test section

The flow induced vibrations are measured with the help of an accelerometer and a laser vibrometer. The piezoelectric accelerometer, whose resonance frequency is 54 kHz, is fitted on the profile support and a portable laser vibrometer is used to survey the hydrofoil surface vibrations. The measurement principle of the laser vibrometer is based on the detection of the frequency shift of the reflected laser beam according to the Doppler effect; the frequency shift being directly related to the displacement velocity of the surface in the laser direction. The location of the vibration amplitude measurements points is shown in Figure 3. Hydrofoil vibration measurements are synchronized with the accelerometer signal used as the reference. The amplitude and the phase of the hydrofoil motion at each measurement point are obtained and the eigen mode is identified for the detected hydro-elastic coupling.

The data acquisition system has 16 bits A/D resolution, 16 inputs, a memory depth of 1 MSamples/Channel and a maximum sampling frequency of 51.2 kHz/Channel.

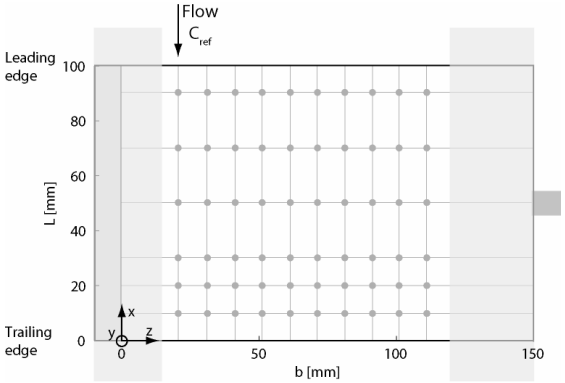

Figure 3 : Location of the hydrofoil vibration amplitude measurements points

NUMERICAL SETUP

The computational domain is the equivalent 2D test section of the hydrodynamic tunnel. The domain is constructed of three rows of mesh in the spanwise direction with symmetry conditions at its border. The whole mesh generation process is carried out with the help of the ICEMCFD5 software. The modeled domain and the used structured mesh are defined in Figure 4. The number of mesh nodes is 150'000 and the values of the first grid points off the wall remain about y+=1. The boundary conditions and the numerical configuration are defined in Table 1 and 2 respectively.

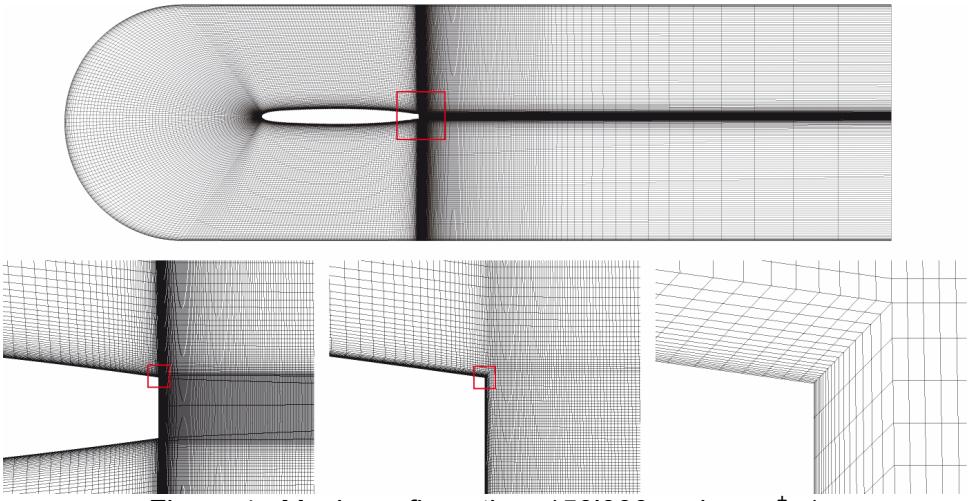

Figure 4 : Mesh configuration, 150'000 nodes, y^+=1

Table 1: Boundary conditions

Boundary conditions	**Simulation type**
Inlet	Cartesian velocity (C_{ref}=10, 16, 20, 24 m/s)
Outlet	Average static pressure
Solid surfaces	Non slip wall, Log. law model

Table 2: Numerical configuration

Resolution scheme	**Turbulence model**	**Convergence**
Spatial discretisation: 2nd order (Blend factor=1.0) Time discretisation : Euler, 2nd order backward t= $2.0 \cdot 10^{-5}$	SST	Max. Residuals = 10^{-4} 10 inner coef loops

RESULTS

Experimental vortex shedding frequency and fluid structure interaction

The spectra of the laser vibrometer signals are presented in Figure 5 left in a waterfall plot for different upstream velocities. Most of the spectral energy is concentrated around a frequency which increases with the upstream velocity. We have identified this frequency as the shedding frequency of Kármán vortices. The amplitude of the induced vibration changes according to the upstream velocity: As the vortex shedding frequency approaches one of the natural frequencies of the combined fluid-structure system, the coupling takes place with a significant increase of noise and vibration levels. The vortex shedding frequency is locked onto the structural eigen frequency, which is 900 Hz, for flow velocity ranging from 11 to 13 m/s, i.e. Re_h =35'000 to 42'000. In addition to the energy at the vortex shedding frequency, all the spectra include energy at this eigen frequency.

The vortex shedding frequencies normalized by the lock-in frequency and derived from the laser vibrometer and the accelerometer signals are presented in Figure 5 right as a function of the flow velocity. The presented two evolutions are virtually identical. A linear relationship between the vortex shedding frequency and the upstream velocity is observed as far as none of resonance frequencies of the hydrofoil is excited; the generation process of Kármán vortices follows the Strouhal law with a mean value of 0.24 for *St*. The hydrofoil trailing edge vibration amplitude at the vortex shedding frequency is also evidenced in Figure 5. In lock-in conditions corresponding to 11-13 m/s upstream velocities, we observe the increase and decrease of the vibration amplitude.

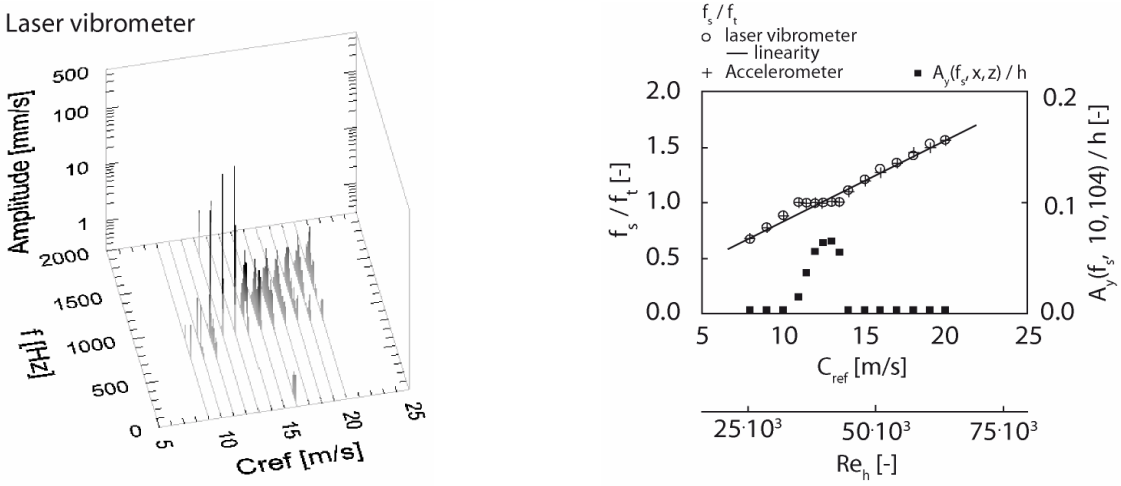

Figure 5 : For different upstream velocities (Left) Spectra of the laser vibrometer signals (Right) Shedding frequency of Kármán vortices and vibration amplitude of the hydrofoil trailing edge

For the above-mentioned lock-in condition, the hydrofoil surface vibration is surveyed by laser vibrometer measurements. As illustrated in Figure 6, the modal shape is identified as the 1st torsion mode. The maximum vibration amplitude of the trailing edge is up to $0.2.10^{-3}$ m. In this case, the vibration is found to be large enough to dominate the unsteady flow field and a self-controlled vibration is induced.

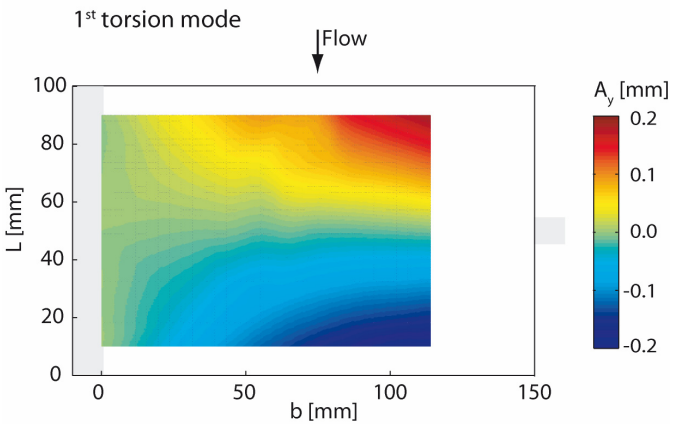

Figure 6: Survey of the hydrofoil surface vibration amplitude for lock-in condition, C_{ref}= 12 m/s

Computation results and validation

The computed value of the lift coefficient during a simulation is reported in Figure 7. From the jet flow configuration (steady state computation), the Kármán instability takes place after few iterations and converge to a fully periodic flow with discrete roll-up and shedding of vortical structures.

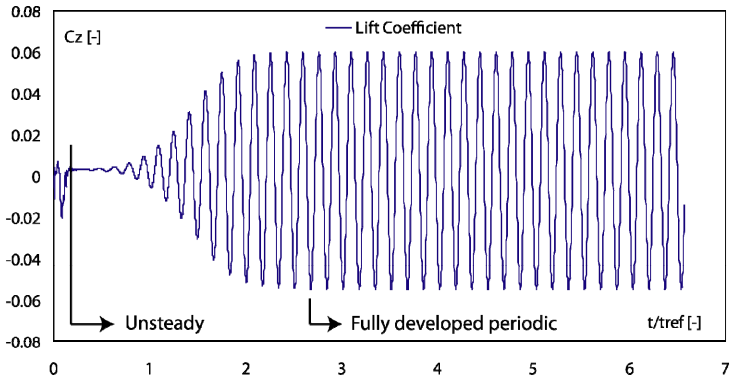

Figure 7: Lift coefficient history C_{ref} =16m/s

The spanwise vorticity field of the numerical simulations is shown in Figure 8 and illustrates the shed vortices. It is characterized by regions of high vorticity fields with alternate sense of rotation, with an upper row of negative vortices (black) and lower row

of positive vortices (white). The numerical solution exhibits a strong vorticity diffusion in the near wake of the hydrofoil.

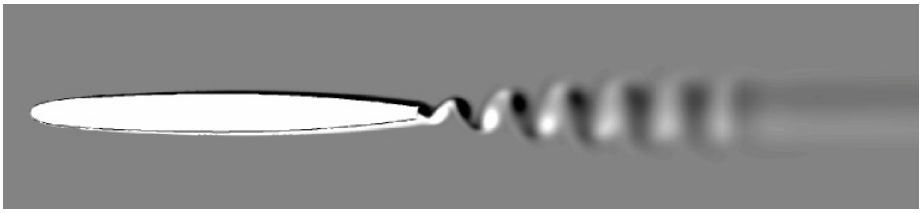

Figure 8: Computed spanwise vorticity, positive: white, negative: black

The measured and computed values of vortex shedding frequency for different upstream velocities are reported in Figure 9. A linear relationship between the shedding frequency and the upstream velocity is observed in both cases, which is in agreement with the Strouhal law. Nevertheless, the Strouhal number mean values are *St*=0.24 for the measurements and *St*=0.19 for the numerical simulations leading to a numerical underestimation of about 20%.

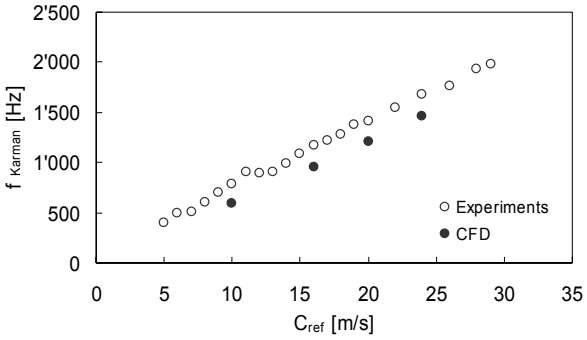

Figure 9: Experimental and computational shedding frequency of Kármán vortices vs the reference velocity

The above-mentioned underestimation occurs for all of the investigated numerical configurations. No significant influence of the turbulence models and the incoming flow turbulence intensity is observed on the computed values. The vortex shedding frequency remains also constant when the mesh size is increased from 10’000 to 150’000 elements or the near wall mesh resolution (y+) is decreased from 20 to 1.

Vortex shedding from bluff bodies does not occur at a single distinct frequency, but rather it wanders over a narrow band of frequencies with a range of amplitude and it is not constant along the span. The spanwise variations in the flow can be understood when vibration signal traces are considered, Figure 10 left. For lock-off condition, the time trace displays amplitude modulation and weak shedding cycles, which are typical

of the occurrence of vortex street dislocations. The cavitation allows the visualization of the turbulent wake flow. The top-view photographs evidence the vortices distortions and dislocations, Figure 10 right.

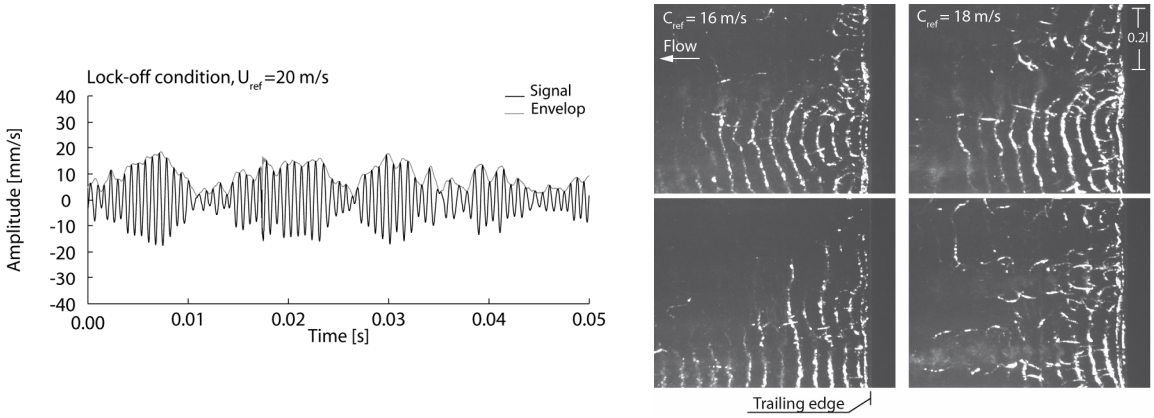

Figure 10: Signal traces of the laser vibrometer and top-view photographs of cavitating Kármán vortex street in lock-off conditions

Since 3D instability of Kármán vortices is observed experimentally, 3D computation of the same case study is carried out by performing an extrusion of the 2D mesh through 75 slices to reach the configuration of 150mm of span. A bi-geometric law evolution is used to ensure correct *y+* value on the side walls. The time history of the computed lift coefficient is reported in Figure 11 left. The signal exhibits fluctuations at the Strouhal frequency with a strong modulation which is similar to the flow induced vibration signal. According to the vorticity field at the lower side of the trailing edge, the vortices 3D instability is well predicted. Nevertheless, no significant improvement of the shedding frequency by the 3D computations is achieved: The 3D computations underestimate the measured values of 20%.

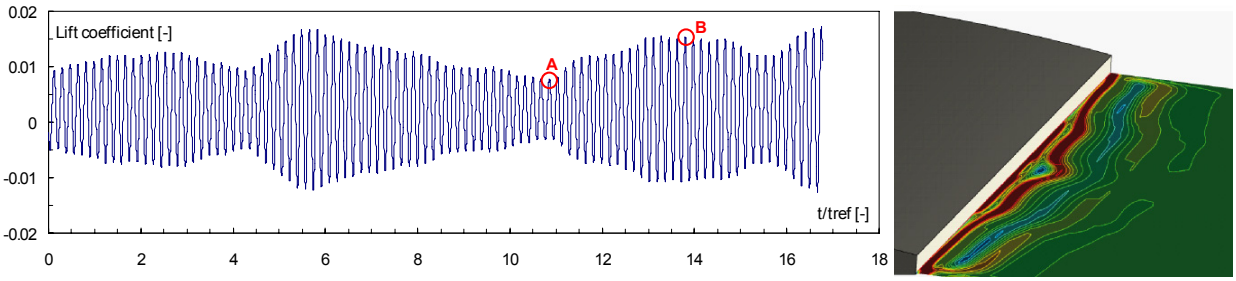

Figure 11: Lift coefficient time history for the 3D SST computations and vorticity field at the lower side of the trailing edge

Experimental setup modification: Hydrofoil embedding effects

To investigate the issue of discrepancy between absolute values of measured and computed shedding frequency, we intend to address the effect of the fluid structure interaction. In the experimental configuration, the hydrofoil is embedded on one side while it is pivot embedded on the other side. This configuration leaves freedom to the hydrofoil to oscillate in torsion mode. Despite the low level of vibration outside the lock-in conditions, one may question the effect of such vibration on the generation mechanism of Kármán vortices. We modify the experimental case study by embedding both sides of the hydrofoil, Figure 12, in order to significantly reduce the vibration level and the subsequent fluid structure interaction.

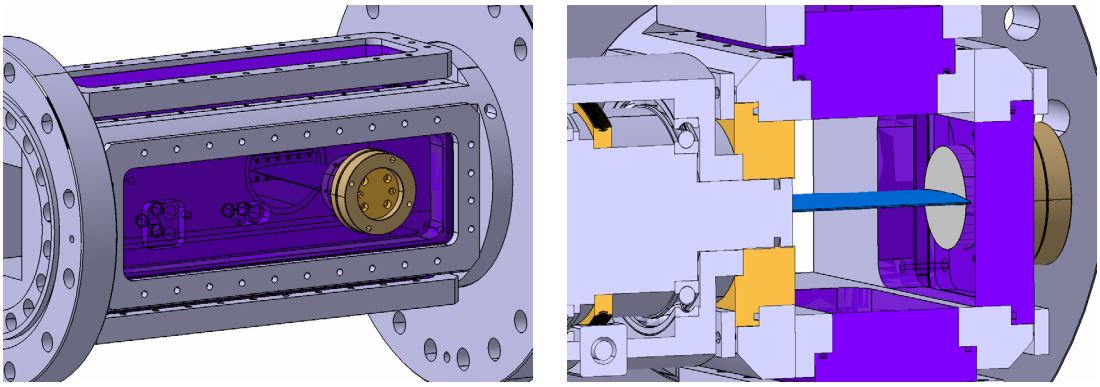

Figure 12 : Hydrofoil embedment in the test section

The vortex shedding frequencies derived from the flow-induced vibration measurements are presented in Figure 13 as a function of the flow velocity. According to the hydrofoil embedment modification, the eigen frequencies and modes have changes. The lock-in of the shedding frequency in a range of upstream velocity does not occur anymore. Nevertheless, no significant modification of the vortex shedding frequency is obviously observed for the two configurations. The hydrofoil vibration is thus not the source of the CFD underestimation.

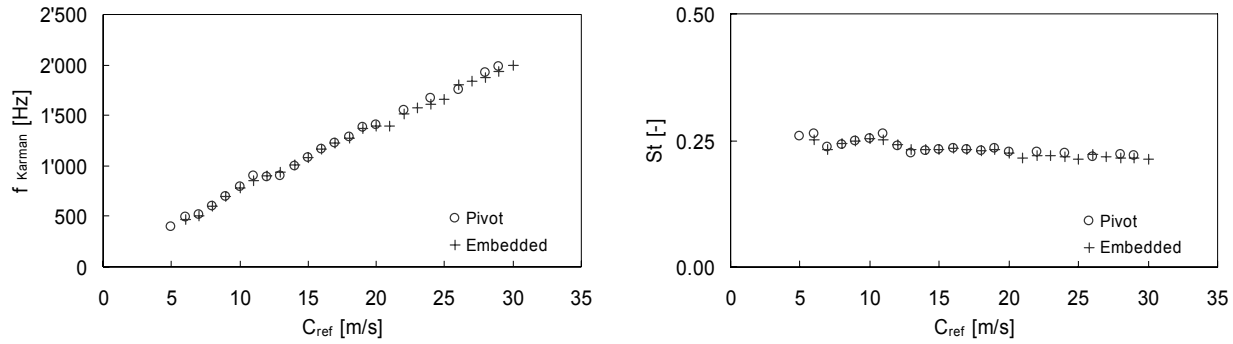

Figure 13: Vortex shedding frequency and Strouhal number vs the reference velocity for the two hydrofoil mountings

Experimental setup modification: Roughness effects

The Kármán vortices involve the interaction of three shear layers; the boundary layer, the separating free shear layer and the wake. Boundary layer transition to turbulence is a consequence of the adverse pressure gradient that exists past the minimum pressure location. Using miniature wall pressure sensors on the hydrofoil, Caron [5] evidences that the boundary layer transition point to turbulence for this profile geometry is located slightly downstream of the midchord for an incidence angle of 0°. In contrast, the numerical simulation, as it solves the RANS equations, models the whole flow as being turbulent. In order to investigate the sensitivity of the vortex shedding frequency to the boundary layer, rough stripes, made of glue and 150 μm diameter sand, are placed just behind the hydrofoil leading edge, Figure 14. The average thickness of the rough spots *k* is 0.2 mm leading to a relative roughness *k/d* of 0.06. For such a configuration, the boundary layer is turbulent from the leading edge in a similar way to the computations.

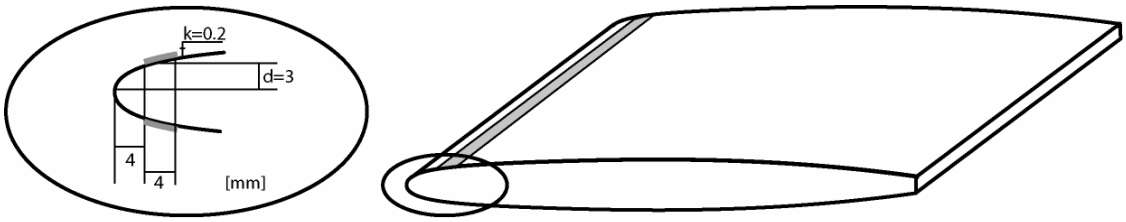

Figure 14 : Sketch of the rough stripes at the hydrofoil leading edge

The vortex shedding frequencies are presented in Figure 15 as a function of the flow velocity. Notable influence of the rough stripes on the frequencies is observed: The vortex shedding frequencies are significantly decreased in comparison to the smooth leading edge. The average Strouhal number *St* decreases from 0.24 to 0.18 and is nearly equal to the computational one, *St*=0.19. Kármán vortices being very sensitive to the boundary layer, differences in the transition points between experiments and computations have to be minimized in order to aspire good agreement.

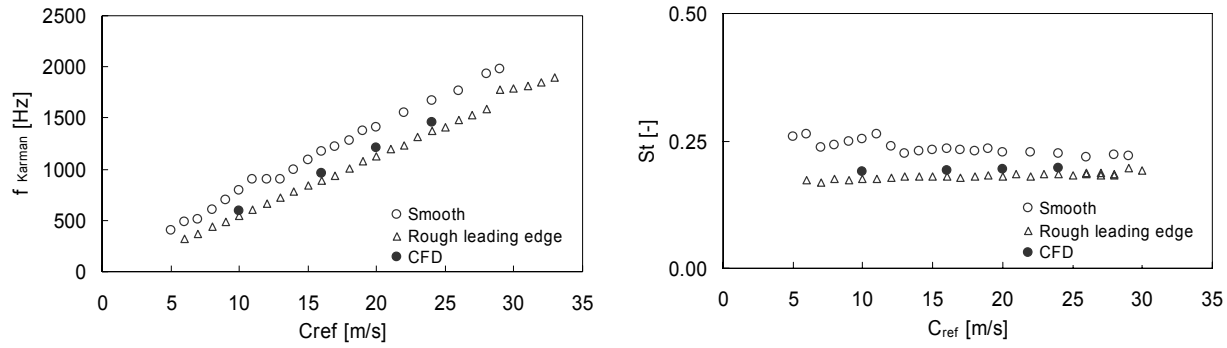

Figure 15: Vortex shedding frequency and Strouhal number vs the reference velocity for the two hydrofoil roughness

CONCLUSION

The Kármán vortices generated in the wake of a 2D hydrofoil at high Reynolds number, i.e. Re_h=25·10^3-65·10^3, are investigated in the EPFL high speed cavitation tunnel and numerically simulated.

The vortex shedding frequency, derived from flow induced vibrations measurements, is found to follow the Strouhal law as long as none of the resonance frequencies of the hydrofoil is excited. For such lock-off conditions, the Kármán vortices exhibit a strong spanwise 3D instability. For Reynolds numbers ranging from 35'000 to 40'000, the torsion mode of the hydrofoil is excited with a substantial increase of the vibration level. In this case, the shedding frequency is locked onto the vibration frequency.

The vortex roll-up, shedding and advection are well predicted by the computations as well as the 3D instability. Nevertheless, the numerical simulations underestimate the vortex shedding frequency of about 20%. No significant influence of the turbulence models, the incoming flow turbulence intensity and the mesh size is observed on the computed values. To investigate the issue of discrepancy between absolute values of measured and computed shedding frequency, we intend to address the sensitivity of the vortex shedding frequency to the boundary layer. It is indeed know that the boundary layer transition point to turbulence for this profile geometry is located slightly downstream of the midchord for an incidence angle of 0°. In contrast, the numerical simulation, as it solves the RANS equations, models the whole flow as being turbulent. Consequently, rough stripes are placed just behind the hydrofoil leading edge. For such a configuration, the boundary layer is turbulent from the leading edge in a similar way to the computations. Notable influence of the roughness is observed: The vortex shedding frequencies are significantly decreased in comparison to the smooth leading edge. The average Strouhal number St decreases from 0.24 to 0.18 and is nearly equal to the computational one, St=0.19. Kármán vortices being very sensitive to the boundary layer, differences in the transition points between experiments and computations have to be minimized in order to aspire good agreement.

ACKNOWLEDGMENTS

The investigation reported in this paper is part of the work carried out for the HYDRODYNA, Eureka Research Project n° 3246, whose partners are ALSTOM Hydro, EDF-CIH, EPFL, GE Hydro, UPC-CDIF, VATECH Hydro and VOITH-SIEMENS Hydro Power Generation. The project is also financially supported by CTI the Swiss Federal

Commission for Technology and Innovation, grant CTI n° 7045-1. The authors are very grateful to the HYDRODYNA Technical Committee for its involvement and constant support to the project. Finally the staff of the EPFL Laboratory for Hydraulic Machines should be thanked for its support in the experimental and numerical work.

NOMENCLATURE

A	Inter-vortex spacing in one row [m]	l	Hydrofoil chord length [m]
$A_y(f_s,x,z)$	Hydrofoil vibration amplitude for the shedding frequency f_s at coordinates (x,z) [m]	p_{inlet}	Reference pressure at the test section inlet [bar]
b	Hydrofoil span [m]	Re_h	Reynolds number [-] $Re_h=C_{ref}h/\upsilon$
C_{ref}	Reference velocity at the test section inlet [m/s]	St	Strouhal number [-] $St=f_s h/C_{ref}$
f_s	Vortices shedding frequency [Hz]	h	Hydrofoil trailing edge thickness [m]
f_t	Hydrofoil torsion eigen frequency [Hz]	α	Incidence angle of the hydrofoil [°]
		υ	Kinematic viscosity [m^2/s]

REFERENCES

[1] Achenbach E., Heinecke E. (1981), On vortex shedding from smooth and rough cylinders in the range of Reynolds numbers $6\cdot10^3$ to $5\cdot10^6$, J.Fluid Mech, 1981 (109):239-251

[2] Arndt R. (1976), Semi-empirical analysis of cavitation in the wake of a sharp-edged disk, J.Fluid Mech, 98 (3):560-562

[3] Avellan F. et al. (1987), A new high speed cavitation tunnel, ASME Winter Annual Meeting, Boston (USA), 57: 49-60

[4] Belahadji B. et al. (1995), Cavitation in the rotational structures of a turbulent wake, J.Fluid Mech, 287:383-403

[5] Caron J.-F., Farhat M., Avellan F. (200), On the leading edge cavity development of an oscillating hydrofoil, ASME Fluids Engineering Division Summer Meeting, Boston (USA), FEDSM2000-11016

[6] Davies M.E. (1975), A comparison of the wake structure of a stationary and oscillating bluff body, using a conditional averaging technique, J.Fluid Mech, 75:209-231

[7] Djeridi H., Braza M., Perrin R., Harran G., Cid E., Cazin S. (2003), Near-wake turbulence properties around a circular cylinder at high Reynolds number, J. Flow, Turbulence and Combustion 71:19-34

[8] Gerich D., Eckelmann H. (1982) Influence of end plates and free ends on the shedding frequency of circular cylinders, J.Fluid Mech 122:109-122

[9] Gerrard JH. (1966), The mechanics of the formation region of vortices behind bluff bodies, J.Fluid Mech, 25: 401-413

[10] Gerrard JH. (1978), Wakes of cylindrical bluff bodies at low Reynolds-number, Phil Trans Royal Soc, 288(1354):351

[11] Gilbert S., Sigurdson L. (2005), Hydrogen bubble flow visualization of a self-oscillating cylinder vortex street “void”, Phys. Fluids 17:091104

[12] Pauchet J. et al. (1992), The prediction of cavitation inception in turbulent water jets, Cavitation and Multiphase Flow Forum, SED, 135:149-158

[13] Prasad A., Williamson C.H.K. (1997), The instability of the shear layer separating from a bluff body, J.Fluid Mech, 333:375-402

[14] Rockwell D. (1998), Vortex-body interactions, Annu. Rev. Fluid Mech, 30:199-229

[15] Slaouti A., Gerrard JH. (1981), An experimental investigation of the end effects on the wake of a circular cylinder towed through water at low Reynolds number, J.Fluid Mech, 112:297-314

[16] Sridhar G., Katz J. (1999) Effect of entrained bubbles on the structure of vortex rings, J.Fluid Mech 397:171-202

[17] Tritton DJ. (1959), Experiments on the flow past a circular cylinder at low Reynolds number, J.Fluid Mech, 6:547-567

[18] Williamson C.H.K. (1988), Defining a universal and continuous Strouhal-Reynolds number relationship for the laminar vortex shedding of a circular cylinder, Phys. Fluids , 31:2742

[19] Williamson C.H.K., Roshko A. (1998), Vortex formation in the wake of an oscillating cylinder, J. Fluids Struct, 2:355-381

[20] Williamson C.H.K., Govardhan R. (2004), Vortex-induced vibrations, Annu. Rev. Fluid Mech, 36:413-455

[21] Young J., Holl J. (1966), Effects of cavitation on periodic wakes behind symmetric wedges, J. Basic Engrg, 88:163-176